Boutelier, D. A., Cruden, A. R. (2008): Impact of regional mantle flow on subducting plate geometry and interplate stress: insights from physical modelling. - Geophysical Journal International, 174, 2, pp. 719—732.

DOI: http://doi.org/10.1111/j.1365-246X.2008.03826.x

Geophys. J. Int. (2008) **174,** 719–732 doi: 10.1111/j.1365-246X.2008.03826.x

Impact of regional mantle flow on subducting plate geometry and interplate stress: insights from physical modelling

David A. Boutelier* and Alexander R. Cruden

Department of Geology, University of Toronto, 22 *Russell Street, Toronto,* ON M5S 3B1, *Canada.*

Accepted 2008 April 17. Received 2008 January 16; in original form 2007 July 2

SUMMARY

Physical models of subduction investigate the impact of regional mantle flow on the structure of the subducted slab and deformation of the downgoing and overriding plates. The initial mantle flow direction beneath the overriding plate can be horizontal or vertical, depending on its location with respect to the asthenospheric flow field. Imposed mantle flow produces either over or underpressure on the lower surface of the slab depending on the initial mantle flow pattern (horizontal or vertical, respectively). Overpressure promotes shallow dip subduction while underpressure tends to steepen the slab. Horizontal mantle flow with rates of 1–10 cm yr^{-1} provides sufficient overpressure on a dense subducting lithosphere to obtain a subduction angle of $\sim 60^{\circ}$, while the same lithospheric slab sinks vertically when no flow is imposed. Vertical drag force (due to downward mantle flow) exerted on a slab can result in steep subduction if the slab is neutrally buoyant but fails to produce steep subduction of buoyant oceanic lithosphere. The strain regime in the overriding plate due to the asthenospheric drag force depends largely on slab geometry. When the slab dip is steeper than the interplate zone, the drag force produces negative additional normal stress on the interplate zone and tensile horizontal stress in the overriding plate. When the slab dip is shallower than the interplate zone, an additional positive normal stress is produced on the interplate zone and the overriding plate experiences additional horizontal compressive stress. However, the impact of the mantle drag force on interplate pressure is small compared to the influence of the slab pull force since these stress variations can only be observed when the slab is dense and interplate pressure is low.

Key words: Mantle processes; Subduction zone processes; Dynamics of lithosphere and mantle.

1 INTRODUCTION

The subduction of oceanic lithosphere is believed to produce the main force driving plate motion and flow in the mantle (Elsasser 1971; Forsyth & Uyeda 1975; Zhong & Gurnis 1995; Schellart 2004a,b). The slab pull force, F_{sp}, which results from the negative buoyancy of the subducting lithosphere compared to the asthenospheric mantle was thought to control the dynamics of the subduction system and thereby the geometry of the subducted slab and strain regime in the overriding plate (Uyeda & Kanamori 1979). However, modelling studies have shown that the viscous resistance of the mantle also participates in the dynamics of the system (Griffiths *et al.* 1995; Guillou-Frottier *et al.* 1995; Olbertz *et al.* 1997; Royden & Husson 2006). Old and dense subducting slabs are not systematically steeper than young and less dense slabs but generate more backarc opening and/or subduct faster (Schellart 2004a, 2005; Royden & Husson 2006). This is consistent with statistical analyses of subduction zone parameters showing no correlation between subducting lithosphere age and slab dip angle (Cruciani *et al.* 2005; Lallemand *et al.* 2005). However, such statistical analyses also find no clear correlation between trench motion and the age of the downgoing plate (Jarrard 1986; Heuret & Lallemand 2005; Lallemand *et al.* 2005). Particularly intriguing is the weak correlation between absolute motion of the trench and the age of the slab at the trench (Heuret & Lallemand 2005) which suggests that the trench tends to advance (towards the overriding plate) faster when the age of the slab increases. This contrasts with models that suggest the trench should retreat (towards the subducting plate) faster for constant subducting plate velocity because of slab roll-back generated by high F_{sp} (Schellart 2004a, 2005; Enns *et al*. 2005; Martinod *et al*. 2005; Royden & Husson 2006). This apparent contradiction might be resolved by taking into account the kinematics of the overriding plate, which has been shown to influence the motion of the trench and strain regime in the backarc area as well as the slab geometry (Heuret *et al.* 2007). However, some subduction zones reveal slab geometries that are difficult to explain by the effects of either slab pull force or upper plate motion or both. For example, in northestern

*Now at: GeoForschungsZentrum Potsdam, Telegrafenberg, C223, D-14473 Potsdam, Germany. E-mail: david@gfz-potsdam.de.

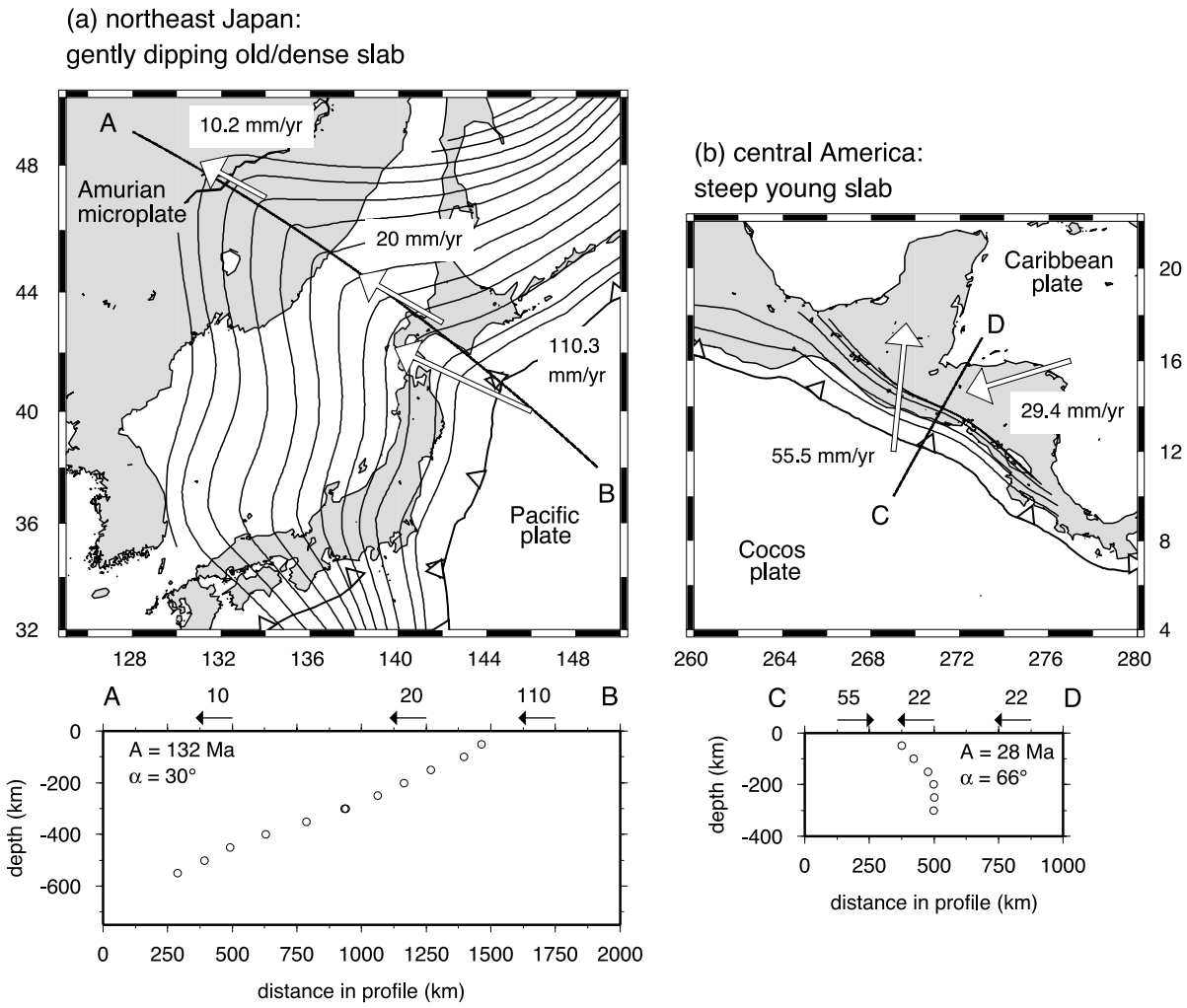

Figure 1. Maps and cross-sections through the subduction zones in northeast Japan (a), and Central America (b). In northeast Japan the old/dense Pacific slab is gently dipping as revealed by the Benioff zone isodepths (Gudmundsson & Sambridge 1998), while in Central America the young Nazca slab is steep. The velocity vectors are HS3-NUVEL1A absolute velocities (Gripp & Gordon 2002). For the Amurian microplate the HS3-NUVEL1A velocity was calculated using GPS velocity data (Heki *et al.* 1999). Ages (A) and slab dip (α) are from the compilation by Lallemand *et al.* (2005).

Japan and Kuril, where the old (∼130 Ma) subducting Pacific lithosphere must have a high slab pull force, the slab is not steep despite its high negative buoyancy and the backarc basin is not opening but closing (Jolivet *et al.* 1995; Taira 2001), (Fig. 1a). One possible explanation for this observation is that the motion of the upper plate and anchorage of the slab in the mantle are responsible for the shallow geometry of the slab and shortening of the backarc area (Griffiths *et al.* 1995; Guillou-Frottier *et al.* 1995; Scholtz & Campos 1995). However, in the HS3-NUVEL1A hotspots reference frame (Gripp & Gordon 2002) both the Eurasian and the Amurian plates are moving slowly away from the trench (advancing, see Fig. 1a), which should promote a steep slab geometry and backarc extension. A third parameter must, therefore, be involved in the dynamics of the subduction system in order to produce a shallow slab and shortening of the backarc domain despite both high F_{sp} and the advance of the overriding plate. Flow in the mantle has been shown to influence the slab geometry (Olbertz *et al.* 1997; Winder & Peacock 2001). A global eastward mantle flow associated with the westward drift of the lithosphere has been proposed to promote shallow dipping east-verging slabs while west-verging slabs would become steeper (Nelson & Temple 1972; Doglioni 1993; Doglioni *et al.* 1999, 2006; Scoppola *et al.* 2006). Although this model predicts the asymmetry of subducted slabs around the Pacific ocean, it does not explain the west-verging shallow subduction in north-eastern Japan and Kuril. Indeed the model also suggests that the subducted lithosphere should be steep at this location because eastward mantle flow would induce an overpressure on the slab upper surface causing a slab-steepening torque. However, westward regional mantle flow could also be due to the reducing volume of the sub-Pacific upper mantle (Garfunkel 1975; Alvarez 1982, 1990, 2001; Garfunkel *et al.* 1986). Westward escape flow under Japan would also alter subduction dynamics and may promote shallow slab geometry due to overpressure on the slab lower surface.

The case of an abnormally steep young slab also exists, for example, in Central America (Fig. 1b) where the young Cocos plate is subducted under the Caribbean plate and slab isodepths (Gudmundsson & Sambridge 1998) reveal a steep slab despite its young age and relatively low negative buoyancy. Furthermore, plate motions cannot explain the steep dip angle of the slab because the Caribbean plate is not moving away from the trench (which would have promoted steep geometry) but towards it (Fig. 1b). This situation also suggests that a third force is acting on the slab, generating the steep geometry, and promoting the neutral strain regime in the overriding plate.

In this study, we employ approximately-2-D scaled laboratory experiments to investigate the influence of horizontal and vertical regional mantle flow on the dynamics of the subduction. We examine whether horizontal flow in the mantle with rates similar to plate motions can generate shallow dipping, dense slabs such as in northeastern Japan (Fig. 1a) and whether vertical flow in the mantle can increase the dip of young slabs such as in Central America (Fig. 1b). In order to investigate the role of the regional mantle flow on subduction dynamics we assume a partial disconnection between the flow in the mantle and the subduction process. It is generally considered that convection downwellings are subducting slabs and, therefore, flow in the mantle is generated by the motion of the slab. In this study we explore the hypothesis that the flow in the mantle around a subduction zone can be horizontal or vertical because of a regional flow (i.e. escape flow) or due to the existence of surrounding subduction zones or sinking slabs (Conrad & Lithgow-Bertelloni 2002; Pysklywec *et al.* 2003; Pysklywec & Ishii 2005). We further assume that the rate of the flow is of the order of plate motion. However, the motion of the slab in our experiments also contributes to changes in the mantle flow pattern and, therefore, mantle flow and subduction are not completely disconnected.

2 MODEL SET-UP

2.1 General modelling scheme

The experiments were carried out in a Plexiglas tank (50 × 20 × 12 cm) filled with transparent, low viscosity polydimethylsiloxane (Clearco Products Co. Pure Silicon 60 000 cSt fluid) that models the asthenosphere/upper mantle (Fig. 2). At the bottom of the tank, a piston translated in a tunnel generates a circulation flow in the tank. The rigid horizontal plate on top of the lower piston (Fig. 2) also represents the boundary between the upper and lower mantle. The overriding and subducting lithospheres, resting on the asthenosphere, are modelled by a single layer of high viscosity polydimethylsiloxane (Dow Corning Co. Silastic 4-2901) mixed with low viscosity silicone polymer and granular fillers (3M Scotchlite Glass Bubbles and talc powder). The subducting plate size is kept constant in all experiments (20 × 11 × 1.2 cm), while different lengths (10–20 cm) of the overriding plate were used to investigate the effects of vertical to horizontal mantle flow around the subducting slab. A short (10 cm) overriding plate allows subduction to occur in the area of the tank where the mantle flow is vertical downward. When a longer (20 cm) overriding plate is used, subduction occurs in the middle of the tank, where mantle flow is horizontal and towards the overriding plate. The interplate zone dip is kept constant in all experiments at 45° (Fig. 2). Subduction is driven by a second piston that pushes the subducting plate at constant rate, a slab-pull force due to the relative density of the slab, and a basal drag force exerted by flow in the model asthenosphere. Side pictures of the experiments record slab structure and mantle flow (visualized using motions of passive markers) while horizontal deformation is studied via passive grids imprinted on top of both plates.

2.2 Scaling

We assume that the lithosphere and asthenosphere are two Newtonian, incompressible and slowly moving fluids. The similarity criteria can be derived from the expression of the stress tensor in a moving fluid:

$$\sigma_{ij} = \eta\left(\frac{\partial v_i}{\partial x_j} + \frac{\partial v_j}{\partial x_i}\right) - p\delta_{ij}, \tag{1}$$

where σ_{ij} is the stress tensor (with $i, j = 1, 2, 3$), η is the dynamic viscosity, v_i are the components of the velocity tensor in Cartesian coordinates x_i, and $-p\delta_{ij}$ is the stress tensor when the fluid is at rest with p the pressure and δ_{ij} Kronecker's delta. Eq. (1) can be non-dimensionalized by substituting for each parameter the product of a reference value (denoted by a tilde) and a dimensionless parameter (denoted by a prime): $x_i = \tilde{x}x'_i$, $v_i = \tilde{v}v'_i, \ldots$ The reference pressure $\tilde{p}$ can be replaced by the product $\tilde{\rho}\tilde{g}\tilde{x}$ and the reference value for stress $\tilde{\sigma}$ can be replaced by the same product for dimensional reasons (Buckingham 1914). Eq. (1) becomes:

$$\tilde{\rho}\tilde{g}\tilde{x}\sigma'_{ij} = \eta'\frac{\tilde{\eta}\tilde{v}}{\tilde{x}}\left(\frac{\partial v'_i}{\partial x'_j} + \frac{\partial v'_j}{\partial x'_i}\right) - \tilde{\rho}\tilde{g}\tilde{x}p'\delta_{ij}. \tag{2}$$

Or dividing by $\tilde{\rho}\tilde{g}\tilde{x}$:

$$\sigma'_{ij} = \eta'\left(\frac{\partial v'_i}{\partial x'_j} + \frac{\partial v'_j}{\partial x'_i}\right)\frac{\tilde{\eta}\tilde{v}}{\tilde{\rho}\tilde{g}\tilde{x}^2} - p'\delta_{ij}. \tag{3}$$

It follows from (3) that all systems having the same values for the dimensionless ratio $\tilde{\eta}\tilde{v}/\tilde{\rho}\tilde{g}\tilde{x}^2$ reduce to the same dimensionless equation and are thus similar systems. Time t does not appear in the obtained criterion, but since we have one velocity v and one length scale x, we can deduce the timescale in the experiments using: $vt/x = \text{Const}$. Finally, because we have two materials but derived the scaling criterion irrespective of the nature of the materials we must add: $\rho_l/\rho_a = \text{Const}$ and $\eta_l/\eta_a = \text{Const}$ where subscripts l and a refer to lithosphere and asthenosphere, respectively. These

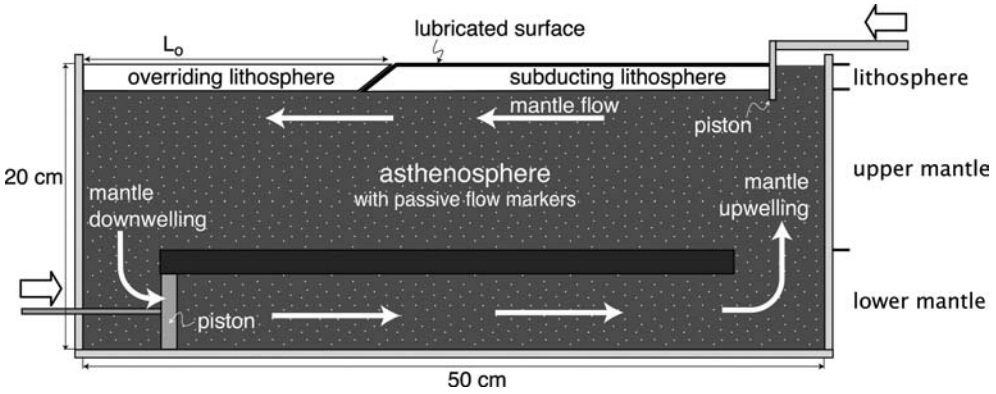

Figure 2. Schematic cross-section of the experimental set-up. Two lithospheric plates made of highly filled silicon polymers rest on the asthenosphere modelled by transparent low viscosity silicon polymer. Flow in the asthenosphere is imposed using the lower piston while the upper piston moves at the same rate and pushes the subducting plate.

last two dimensionless ratios ensure that the scaling of densities and viscosities are homogeneously applied to both materials. The similarity criteria used for the scaling of the experiments are then:

$$\left\{\begin{array}{r} \eta v/\rho g x^2 = \text{Const} \\ vt/x = \text{Const} \\ \rho_l/\rho_a = \text{Const} \\ \eta_l/\eta_a = \text{Const} \end{array}\right\}. \quad (4)$$

2.3 Materials

Rheological properties of the analogue materials were measured using an AR1000 rheometer (TA Instruments) at a variety of shear stresses at room temperature. The silicone polymer used to model the asthenosphere is a Newtonian fluid, while the mixture used to model the lithosphere is viscoelastic (with very little elasticity) and shear thinning: its viscosity decreases with increasing shear stress or shear rate (Fig. 3). Over three orders of magnitude the rheological model that best fits the measured material behaviour is a power law of the form $\dot{\gamma} = \tau^n/\eta$ where $\dot{\gamma}$ is the shear rate, τ is the shear stress, η is the material viscosity coefficient and n is the power-law exponent equal to 1.6. This exponent is far below the power-law exponent determined for diffusion creep of olivine which ranges between 3 and 3.5 (Karato & Wu 1993). For scaling purposes, we therefore, used the effective viscosity at the typical experimental strain rate (3×10^{-3} s^{-1}; Fig. 3). High stress dynamic processes that may occur in the experiment (e.g. slab break-off) will, therefore, have an underestimated rate since the analogue material cannot weaken as much as the natural oceanic lithosphere.

The density of the model asthenosphere is constant in all experiments (975 kg m^{-3}) while the density of the model lithosphere can be varied to investigate the effects of the slab pull force. Different densities are obtained by changing the ratio of the two granular fillers in the lithosphere material. The filler volume fraction is kept constant and the effective viscosity is not changed.

To obtain plate-like deformation with the viscous material used to model the lithosphere, we lubricate the upper surface of the subducting plate. Our viscous material is not intrinsically strain softening and, therefore, strain localisation in the subduction zone has to be induced by lubricating the subducting plate upper surface with a 0.5-mm-thick layer of low viscosity silicone. The vertical sides of the plates are not lubricated before being put in the experimental tank. The model lithospheres are slightly narrower than the experimental tank and a 5 mm gap between the lithospheres and the side walls of the tank is filled by the low viscosity silicone modelling the asthenosphere which acts as a lubricant.

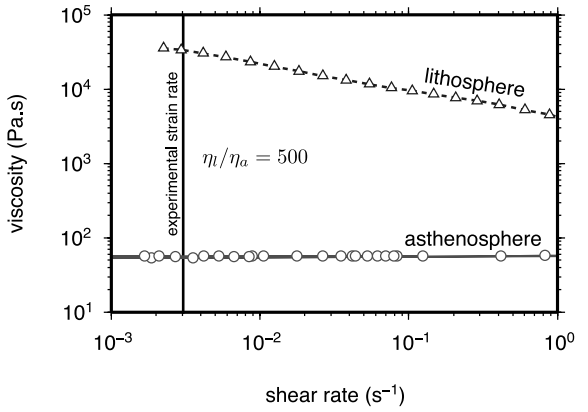

Figure 3. Effective viscosity versus shear rate diagram for the materials used to model the lithosphere and asthenosphere. The silicone polymer used for the asthenosphere is a Newtonian fluid while the mixture used for the lithosphere is shear thinning, its viscosity decreases with increasing shear rate. At the experimental shear rate the ratio of the effective viscosities η_l/η_a is 500.

2.4 Scaling factors

The silicone polymer used to model the asthenosphere has a viscosity of 57 Pa s which represents a viscosity of 1×10^{20} Pa s in nature (Mitrovica & Forte 2004). Our lithosphere is chosen to be ∼500 times more viscous than the asthenosphere. Our model lithosphere is thus 2.8×10^4 Pa s which corresponds to $\sim 5 \times 10^{22}$ Pa s in nature. Using the low viscosity silicon polymer to model the asthenosphere we also set the scaling factor for density: the mantle density is 975 kg m^{-3} in the model which corresponds to 3250 kg m^{-3} in nature. The model lithosphere density is chosen according to the density scaling factor and the prototype lithosphere density. However, in nature the oceanic lithosphere density increases with age. We used a typical value of 1.025 for the ratio of the old lithosphere density over asthenosphere density, corresponding to density difference of ∼80 kg m^{-3} (Cloos 1993). The values of the parameters used in the presented experiments, their equivalents in nature and the scaling factors are presented in Table 1.

3 RESULTS

20 experiments were carried out. Here we report on six experiments that reveal different first order slab geometries and behaviours obtained by varying the mantle flow pattern, density of the subducting lithosphere and boundary conditions (i.e. using the upper or lower piston or both). Table 2 lists the parameters employed in the experiments presented here.

In each experiment, flow in the upper mantle was tracked by following the trajectories of neutrally buoyant particles in sequential side view digital images. For each experimental step presented here, the trajectories plotted are the motions of all tracked particles since the previous step (e.g. Fig. 4c at 1680 s shows trajectories from 840 to 1680 s). Since all the particles in the tank are tracked irrespective of location, the trajectories are 2-D projections of 3-D particle paths. Hence some upward and downward moving trajectories that appear to cross each other are of particles in different vertical planes and/or incorporate various sideways movements, towards or away from the side boundaries.

The deformation of the plates is recorded via passive marker grids imprinted on the top of both plates. Evolution of the horizontal strain is presented in order to characterize the influence of the slab geometry on the strain regime in the overriding and subducting plates. The cumulative convergence and trench parallel normal strains are calculated for each plate from the grids on successive surface images (Fig. 5). ΔL_s and ΔW_s are the cumulative percentage strains of the subducting plate in the convergence parallel and trench parallel directions, respectively, and ΔL_o and ΔW_o are the corresponding percentage strains in the overriding plate.

3.1 Experiment 1: neutrally buoyant slab with vertical mantle flow

In this experiment (Fig. 4) the lithosphere is almost neutrally buoyant (only 0.5 per cent denser than the asthenosphere; Table 2). The

Table 1. Parameter values used in the experiment and scaled to nature. The lithosphere viscosity is the effective viscosity at the experimental strain rate. Scaling factors are the ratios of the values in nature over the values in the experiments.

Parameter	Symbol	Experiments	Nature	Scaling factor
Asthenosphere viscosity	η_a	57 Pa s	1×10^{20} Pa s	1.75×10^{18}
Lithosphere viscosity	η_l	2.8×10^{4} Pa s	4.9×10^{22} Pa s	1.75×10^{18}
Asthenosphere density	ρ_a	975 kg m^{-3}	3250 kg m^{-3}	3.33
Lithosphere density	ρ_l	970–1000 kg m^{-3}	3233–3333 kg m^{-3}	3.33
Lithosphere thickness	H_l	1.2×10^{-2} m	7×10^{4} m	5.8×10^{6}
Plate velocity	V	3.9×10^{-5} m s^{-1} (14.1 cm hr^{-1})	2.54×10^{-9} m s^{-1} (8 cm yr^{-1})	6.5×10^{-5}
Time	t	60 s	5.4×10^{13} s (1.72 Ma)	9×10^{11}

Table 2. Parameters investigated in the presented experiments.

	ρ_l(kg m^{-3})	L_o (cm)	V (cm hr^{-1})	V_m (cm hr^{-1})
Experiment 1	980	10	14	14
Experiment 2	975	20	14	14
Experiment 3	1000	20	14	14
Experiment 4	970	10	14	14
Experiment 5	1000	20	No piston	14
Experiment 6	1000	20	14	No piston

Note: ρ_l is the density of the lithosphere, L_o is the length of the overriding plate, V is the velocity of the upper piston imposing the minimum plate convergence rate and V_m is the velocity of the lower piston imposing the flow in the mantle.

length of the overriding plate is 10 cm providing a vertical mantle flow below the overriding plate. After a few centimetres of subduction, the slab enters the downward mantle flow area (Figs 4b–c). The subducting lithosphere then steepens and follows the mantle flow. After 2400 s, the subducting plate detaches from the upper piston and accelerates into the subduction zone (Figs 4d–e and 6). At this stage the tip of the slab is deeply subducted and enters the slot at the bottom of the tank where the mantle flow is faster. At the end of the experiment, the tip of the slab is almost vertical in the slot but the shallower part of the slab below the interplate zone maintains a shallow angle.

Surface deformation in the experiment starts with convergence parallel shortening of both plates and little trench parallel extension (Fig. 5b). After 300 s, convergence parallel shortening of the subducting plate stops while shortening of the overriding plate continues at a slower rate. At 2000 s, the subducting plate starts to undergo convergence parallel extension and detaches from the upper piston. This convergence parallel extension phase continues until the end of the experiment and is accompanied by trench parallel shortening. During this phase, the overriding plate continues to undergo convergence parallel shortening and trench parallel extension with a slight increase in rate.

3.2 Experiment 2: neutrally buoyant slab with horizontal mantle flow

In this experiment (Fig. 7) the lithosphere and asthenosphere have the same density (Table 2) so there is no slab pull force. The overriding plate is 20 cm long and the mantle flow beneath the subduction zone is horizontal. As the subducting lithosphere progresses into the asthenosphere, the flow remains shallow around the slab as it progressively rotates upwards and aligns with the flow direction (Figs 7c–d). The slab tip however reveals a more complicated and interesting behaviour. The slab tip rises as it travels in the horizontal mantle flow area (Figs 7b–c). As it enters the region of vertical mantle flow the slab tip bends downward (Fig. 7d–f) and eventually reaches a dip angle of 50° at 5100 s. Closer to the interplate zone, the neutrally buoyant slab remains horizontal.

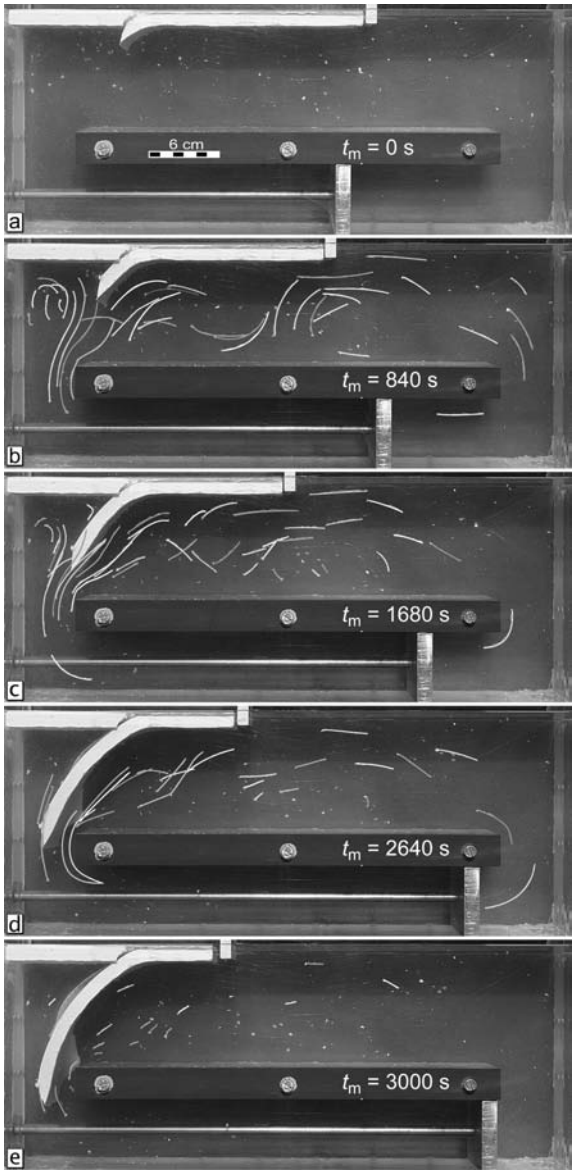

Figure 4. Photographs of the successive stages of Experiment 1, in which the lithosphere is slightly denser than the asthenosphere and the flow in the asthenosphere below the subduction zone is vertical.

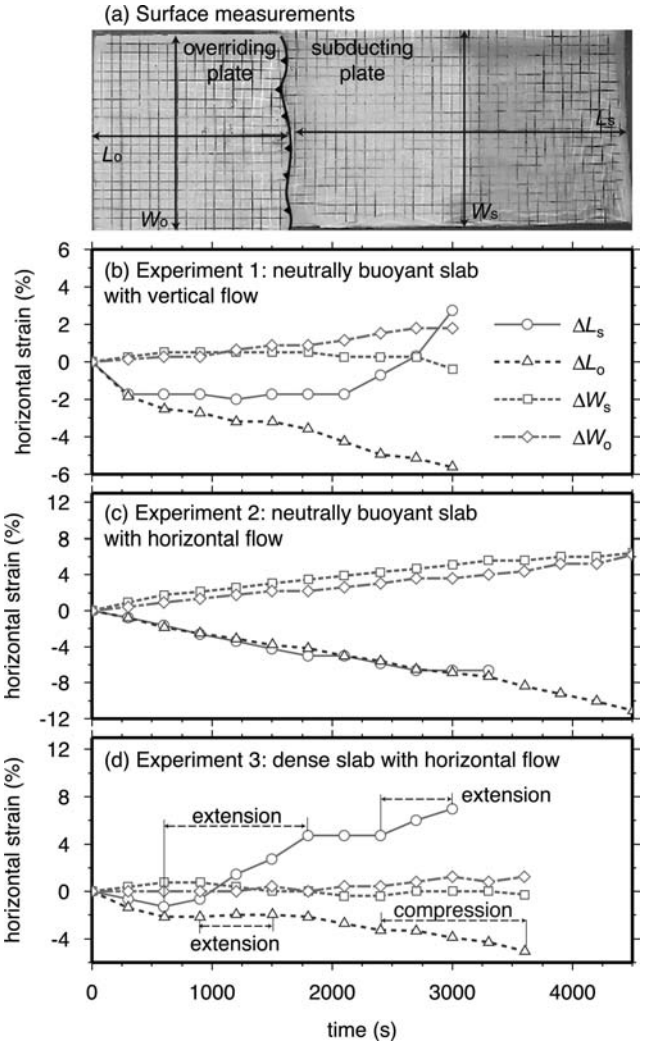

Figure 5. Horizontal deformation of the plates in Experiments 1 (b), 2 (c) and 3 (d). The deformation is measured using grids imprinted on the surface of the plates (a).

Surface deformation of both plates is characterized by convergence parallel shortening and trench parallel extension (Fig. 5c). The strain rates experienced by both plates are very similar and are constant during the experiment (Fig. 5c).

3.3 Experiment 3: dense slab with horizontal mantle flow

In this experiment (Fig. 8) the lithosphere is 2.5 per cent denser than the asthenosphere (Table 2), and the overriding plate length is 20 cm, providing a horizontal mantle flow below the interplate zone. The subducting plate enters the asthenosphere with a dip of 45° that increases as the slab penetrates deeper into the asthenosphere, reaching 60° at 1140 s (Fig. 8b). The slab dip then slowly reduces, going back to 45° at 1800 s (Fig. 8c). The convergence rate then increases as the subducting plate detaches from the upper piston and is pulled into the asthenosphere (Figs 6 and 8d). When the slab touches the lower mantle, it starts to roll over its tip (Figs 8d–e). This process results in a further decrease of the slab dip, which finally reaches 30° at 3780 s (Fig. 8e).

Surface grid deformation in this experiment reveals contrasting strain histories for the subducting and overriding plates. At the beginning of the experiment, subduction initiation results in convergence parallel shortening of both plates and little trench parallel extension (Fig. 5d). The subducting plate then undergoes convergence parallel extension between 1100 and 1700 s, when the plate detaches from the upper piston and accelerates into the subduction zone (Figs 5d and 6). During the same period, shortening of the overriding plate stops and the plate experiences minor convergence parallel extension. Once the subducting plate detaches from the upper piston, it records no further extension while convergence parallel shortening resumes in the overriding lithosphere. When the slab touches the rigid plate at the base of the asthenosphere, at 2400 s, convergence parallel extension resumes in the subducting plate while shortening in the overriding plate continues without any noticeable change in rate.

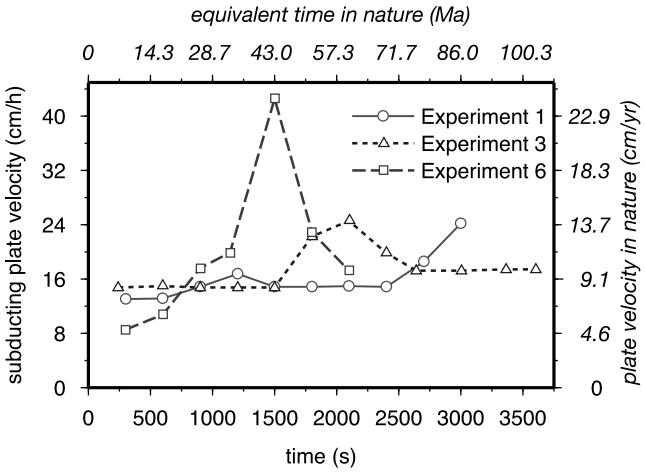

Figure 6. Velocity of the subducting plate versus time in Experiments 1, 3 and 6 with equivalent time and velocities in nature. In Experiments 1 and 3 the plate velocity is imposed with the upper piston but the plate detaches and velocity increases. In Experiment 6, the plate convergence is not imposed with the upper piston but with flow in the asthenosphere and slab negative buoyancy.

3.4 Experiment 4: buoyant slab with vertical mantle flow

In this experiment (Fig. 9) the lithosphere is slightly less dense than the asthenosphere (Table 2). The overriding plate length is 10 cm, so the mantle flow below the overriding plate is vertical. At the beginning of the experiment, the subducting lithosphere moves down with the mantle flow (Figs 9a–c). The subducting slab develops a maximum dip of 40° at 1380 s and it never becomes steeper than the interplate zone. After 1560 s the slab stops going downward and starts to move up and under the overriding plate due to continued compression from the upper piston (Figs 9d–e), although mantle flow below the slab remains downward. The experiment was stopped when the subducted slab underplated the overriding plate.

The surface strain of both plates is similar in both convergence parallel and trench parallel directions (Fig. 10a). Both plates undergo significant and rapid convergence parallel shortening and trench parallel extension. The deformation rate progressively slows down as the downgoing slab starts to underplate the overriding plate (Figs 9c and 10a). At this point convergence parallel shortening of the overriding plate ceases and the shortening rate of the subducting plate is reduced. A strain rate reduction is also observed for the trench parallel extension of both plates. The very high value

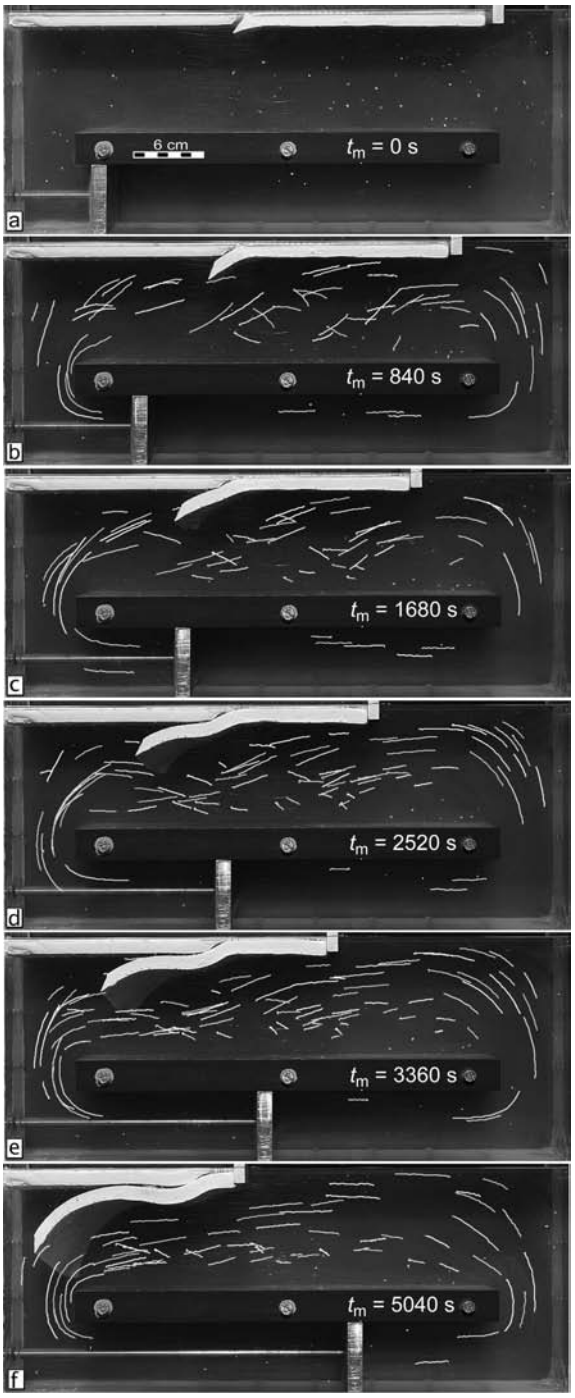

Figure 7. Photographs of the successive stages of Experiment 2, in which the lithosphere is neutrally buoyant and the flow in the asthenosphere below the subduction zone is horizontal.

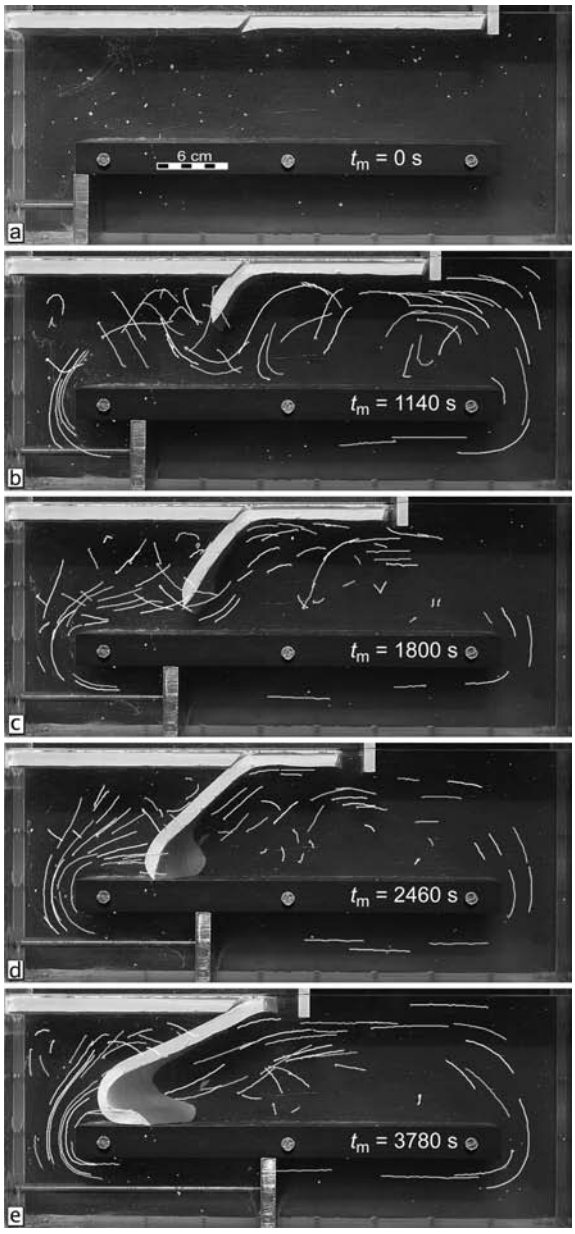

Figure 8. Photographs of the successive stages of Experiment 3, in which the lithosphere is denser (2.5 per cent) than the asthenosphere and the flow below the subduction zone is horizontal.

(∼8 per cent) of ΔW_o and ΔW_s suggests the decrease of the deformation rates is related to the plates reaching the maximum width (the width of the experimental tank).

3.5 Experiment 5: dense slab with no imposed mantle flow

Experiment 5 (Fig. 11) is similar to Experiment 3 (Fig. 8) except that mantle flow is not imposed by the lower piston but results solely from the motion of the subducting plate. The slab tip quickly becomes very steep once it enters the asthenosphere and at 1800 s the slab tip is already vertical (Fig. 11c). The flow in the mantle follows a large-scale circulation cell whose upper part is the lower surface of the subducting plate (Figs 11b–e). A second circulation cell is also produced below the overriding plate (Fig. 11d), but both the dimension of this cell and its rate of the flow are smaller than below the moving subducting plate. When the slab touches the lower mantle boundary, it bends backward and then starts to roll over its tip. The roll over in this experiment is different from that observed in Experiment 3 since the slab tip moves backward along the upper–lower mantle boundary, as it is entrained in the backflow generated by the plate motion (Fig. 11d).

Both plates undergo convergence parallel shortening and trench parallel extension from the beginning of the experiment until 1000 s (Fig. 10b). Then they both experience convergence parallel

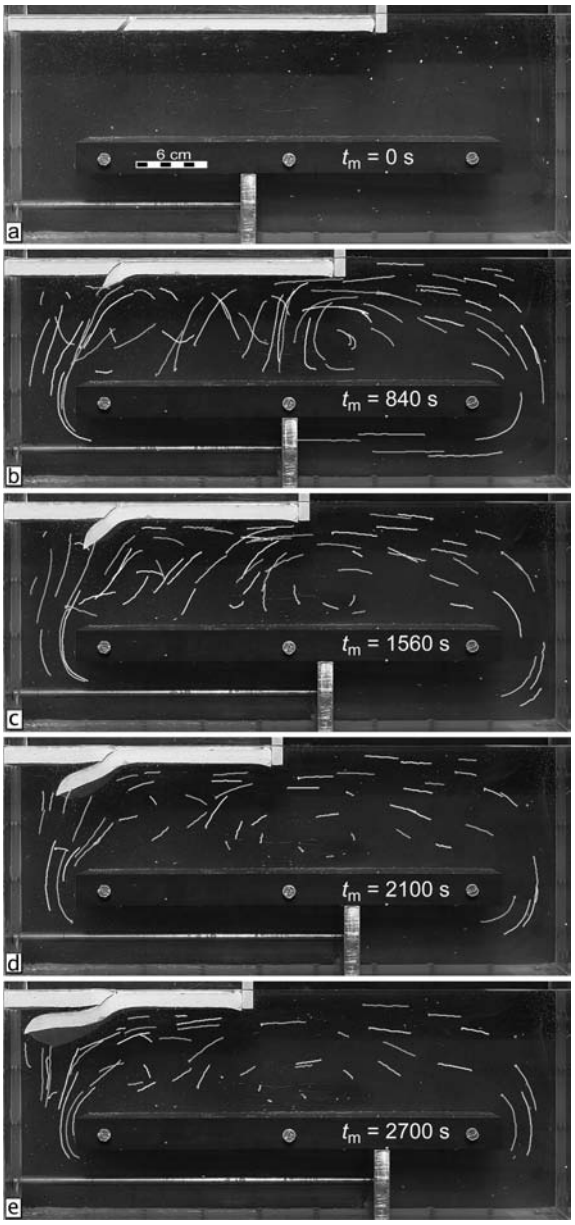

Figure 9. Photographs of the successive stages of Experiment 4, in which the lithosphere is slightly less dense than the asthenosphere and the flow in the asthenosphere below the subduction zone is vertical.

extension until the slab touches the lower mantle boundary at 2500 s. At this point the subducting plate undergoes a stronger convergence parallel extension while the overriding plate is now submitted to convergence parallel shortening. Trench parallel deformation of the plates shows little variation after 1000 s.

3.6 Experiment 6: dense slab, horizontal mantle flow and no imposed plate convergence

Experiment 6 (Fig. 12) is similar to Experiment 3 (Fig. 8) except that no upper piston imposes the plate convergence. The slab pull force and later the slab pull and mantle drag forces drive the subduction process. In the first part of the experiment, the subduction dynamics is driven only by the slab pull force, which also controls the subducting slab geometry. During that period, the subduction

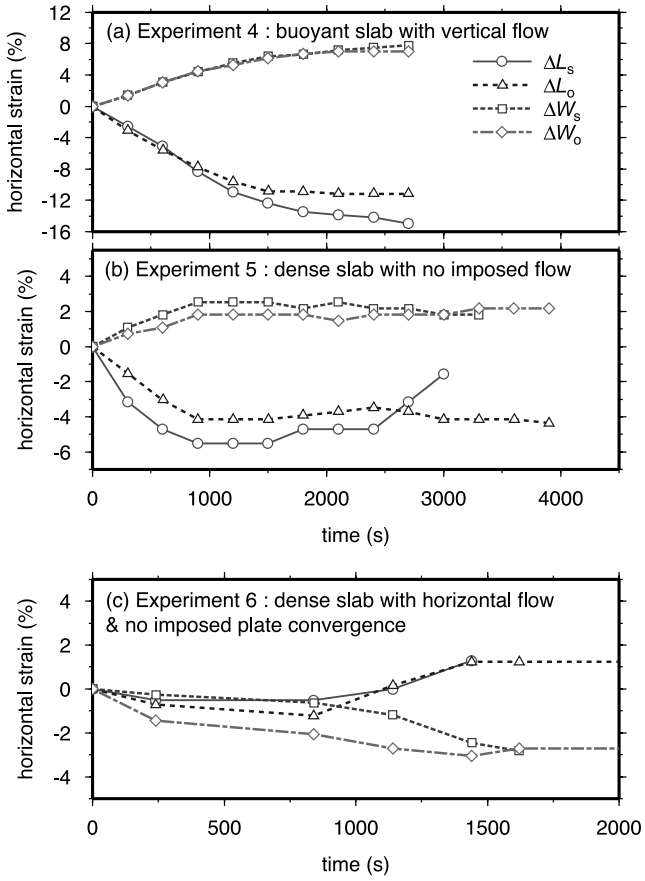

Figure 10. Horizontal deformation of the plates in experiments 4 (a), 5 (b) and 6 (c). See text for discussion.

rate is higher than in any other experiment (Fig. 6). At 1500 s a very steep subducting slab is developed. At this point a horizontal mantle flow was imposed to investigate its influence on the steep slab. The behaviour of the slab in response to the imposed mantle flow is very similar to that observed in Experiment 3 in that it bends forward towards the overriding plate. When the subducting slab touches the lower mantle boundary, it does not roll backward as in Experiment 5 (Fig. 11) but forward as in Experiment 3 (Fig. 8). A unique feature observed in this experiment only is the occurrence of slab retreat or trench rollback. When the slab rolls over (Figs 12d–e), the overriding plate detaches from the back wall of the tank and moves towards the subducting plate. The location of the detachment reflects the simplification we made in assuming the overriding plate has a constant thickness. With this set up, there is no weak zone in the plate except for the contact between the plate and the back wall where some low viscosity silicone polymer infiltrated during model set up. Despite the unusual location, this detachment indicates a tensile horizontal stress in the overriding plate.

Convergence parallel tensile stress in the overriding plate is confirmed by the strain measurements; after 800 s both plates undergo convergence parallel extension. However, the deformation of the plates in this experiment is clearly 3-D since at the beginning of the experiment we observe shortening of both plates in both convergence parallel and trench parallel directions (Fig. 10c). Even though both plates undergo convergence parallel extension and trench parallel shortening after 800 s, the small trench parallel deformation observed suggest that the strain regime is still 3-D.

Figure 11. Photographs of the successive stages of Experiment 5, in which the lithosphere is denser (2.5 per cent) than the asthenosphere and no flow is imposed in the asthenosphere (no lower piston).

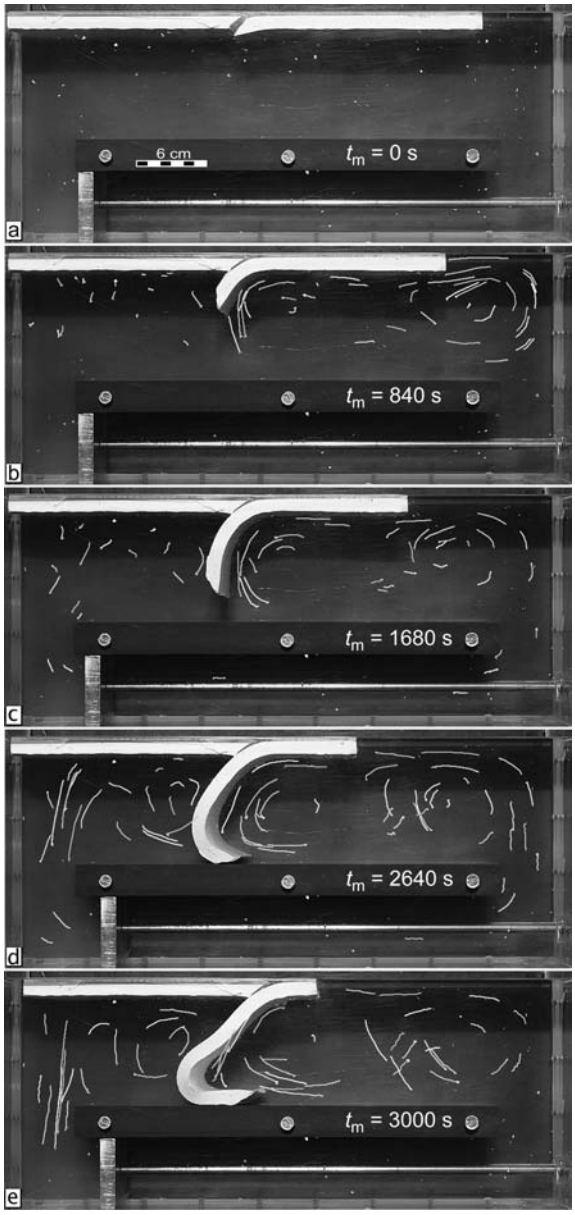

Figure 12. Photographs of the successive stages of Experiment 6, in which the lithosphere is denser than the asthenosphere and the flow in the asthenosphere below the subduction zone is horizontal. In this experiment, the plate convergence rate is not imposed with the upper piston.

4 DISCUSSION

4.1 Impact of mantle flow on slab geometry

In many analogue models of subduction process (Funiciello *et al.* 2003a; Schellart 2004a,b; Bellahsen *et al.* 2005), the overriding plate is weak, usually modelled by asthenosphere material. This corresponds to the case of oceanic subduction when an active backarc spreading centre is present in the overriding plate. In our experiments, trench motion is not precluded but in order for the trench to move, the strong overriding plate must either deform or detach. Consequently, we observe little displacement of the trench (except Experiment 6, Fig. 12), which corresponds to the case of an overriding plate without a backarc spreading centre. Since, the motion of the trench is small, for a given (imposed) convergence rate, the geometry of the slab is mainly controlled by the slab pull force and imposed flow in the mantle. Experiment 2 (neutrally buoyant subducting lithosphere and horizontal mantle flow, Fig. 7) provides important insights on the impact of mantle flow on slab geometry. As there is no slab pull force, the force due to the asthenospheric flow around the slab is the main control on slab geometry, which rotates and aligns with the flow direction. This is illustrated by the behaviour of the slab tip. This experiment reveals that the imposed mantle flow results in an additional over or underpressure on the slab lower surface. When the mantle flow is horizontal, overpressure is imposed on the slab lower surface, generating a slab lifting clockwise torque. When the flow is vertical, an underpressure is imposed on the slab lower surface, resulting in a counter-clockwise torque. This result is consistent with previous laboratory experiments where the subduction zone and trench were translated horizontally with respect to a static asthenosphere (Griffiths *et al.* 1995;

Guillou-Frottier *et al.* 1995), or where trench motion was produced dynamically by the negative buoyancy of the slab (Funiciello *et al.* 2003a; Schellart 2004a). A similar pattern was also obtained when a background flow with slower rate was imposed in the upper mantle (Olbertz *et al.* 1997; Winder & Peacock 2001). It is, however, important to separate the influence of the trench motion and the influence of the mantle flow. In Experiments 2 and 3, we obtained trench perpendicular shortening of the overriding plates (Figs 5, 7 and 8) while the horizontal flow in the mantle produced shallow slabs. We therefore, have trench advance, which was argued previously to promote steepening of the slab. In our Experiments 2 and 3 (Figs 5, 7 and 8) the impact of relatively fast flow in the mantle is more important than the effect of trench motion and the slabs have shallow dip angles.

If the subducting lithosphere is denser than the surrounding asthenosphere, then the slab is submitted to a vertical downward slab pull force, which will tend to increase the slab dip (at constant convergence rate, with no trench motion). The influence of a strong slab pull force on the subducting plate geometry is shown by Experiment 5, in which the slab becomes vertical before it reaches the bottom of the tank (Fig. 11). However, when the subducting lithosphere is not only submitted to a slab pull force but also to an horizontal mantle flow induced overpressure, as in Experiment 3, the slab never attains such a steep geometry (Fig. 8). The overpressure imposed by the flow on the slab lower surface, therefore, partly counterbalances the slab pull force, resulting in a slab with a dip that is intermediate between the 'flat-slab' geometry obtained when horizontal flow is present and F_{sp} is low (Experiment 2, Fig. 7), and the steep geometry obtained when flow in the mantle is not imposed and F_{sp} is high (Experiment 5, Fig. 11). Despite the high rate of mantle flow in Experiment 3 (same order as the plate motion, i.e. $\sim$8 cm yr^{-1}) the slab keeps a rather steep dip of 60° before reaching the bottom of the tank (Figs 8c–d). To obtain a shallower slab it seems necessary to either decrease the slab pull force or increase the mantle flow induced overpressure.

In Experiment 6 (Fig. 12) the slab dip reduces once subjected to mantle flow induced overpressure. This however occurred a few minutes before the slab tip reached the bottom of the tank and was followed by slab roll back (Figs 12d–e), which then also contributed to producing shallower slab dip.

Although mantle flow induced overpressure can result in shallow dipping, dense slabs, the underpressure induced by vertical downward mantle flow appears to be unable to cause deep subduction of buoyant oceanic lithosphere (Experiment 4, Fig. 9). The downward force exerted by the asthenosphere on the slab is proportional to its surface area while the buoyancy driving the slab upward is proportional to its volume. Therefore, as the slab is pushed down along the interplate zone, the buoyancy force increases faster than the mantle drag force and after few centimetres of subduction the buoyancy force exceeds the drag force and the slab starts moving upward. Experiment 4, therefore, reveals the limit of the vertical mantle drag force when the subducting plate is buoyant. However, if the downgoing plate is neutrally buoyant or just slightly denser than the asthenosphere, as in Experiment 1 (Fig. 4), the underpressure induced by the downward mantle flow provides an additional force that tends to increase the slab dip. In such cases it is possible that a young lithosphere that is not much denser than the asthenosphere can develop a rather steep Benioff zone. This result is in agreement with previous numerical modelling of the impact of mantle avalanches on subduction dynamics (Pysklywec *et al.* 2003; Pysklywec & Ishii 2005). However, we should recall that mantle avalanches are time-dependent processes that may not act on the subducted slab for a long enough period of time to alter the dynamics of the subduction system significantly.

4.2 2-D versus 3-D models

A limitation of the present model study is due to the approximately 2-D set up employed. Experiments are performed in a narrow (12 cm) tank with symmetrical boundary conditions, which is not strictly 2-D. Flow in the model asthenosphere is 3-D despite the narrow geometry, being faster in the centre than along the walls of the tank. This is the reason why we observe 3-D deformation of the plates in Experiment 6, when no upper piston is used to impose plate convergence. The slab pull force and mantle drag force result in convergence parallel shortening of the plates, but the 3-D flow in the mantle below also results in trench parallel shortening. Therefore, extension of the plates is confined to the third dimension and the plates thicken. The vertical component of plate deformation was too small to be precisely measured in our successive side photos. This effect diminishes when using the upper piston, as the motion of the subducting plate is then kept constant along the plate width. However the flow remains 3-D deep in the mantle layer. This is also the reason why the flow we imposed in the mantle has rates similar to the applied plate convergence. The volume displaced by the lower piston is smaller than the volume of the upper mantle in our tank but due to the parabolic velocity profiles in vertical and horizontal sections we obtained rates similar to plate motion (i.e. $\sim$8 cm yr^{-1}).

Ideally, 3-D flow in the asthenosphere should be taken into account, because it has been reported that the flow in the mantle beneath the slab may be parallel to the trench (Russo & Silver 1994). Toroidal flow around the slab has been described in both analogue and numerical models (Funiciello *et al.* 2003a,b, 2004; Schellart 2004a; Stegman *et al.* 2006) and was shown to effect intensely the slab edges when the slab is wide and the whole trench system if the slab is narrow (Schellart *et al.* 2007). This is due to the greater distance that upper mantle must flow around wide slabs. In such cases, and if we exclude the slab edges from our investigation then our 2-D approximation is reasonable. Narrow slabs and slab edges have, therefore, to be ignored in our study. Consequently, the steep subduction of the Cocos plate under the Caribbean plate cannot be described by any of the models presented here. The slab window is too close to ignore the toroidal flow generated by slab motion (Johnston & Thorkelson 1997). However, in northeastern Japan and southern Kuril the anomalous shallow geometry of the slab may result from regional escape flow of the sub-Pacific mantle and the effects of toroidal flow around the slab should be small.

4.3 Impact on tectonic regime

It has been shown previously that slab pull force reduces interplate pressure (Shemenda 1994). If this force is large enough the pressure can become smaller than the hydrostatic pressure, generating a tensile horizontal stress in the overriding plate resulting in arc failure and backarc opening (Shemenda 1994; Scholtz & Campos 1995). In accord with previous results we obtained the largest trench-perpendicular compression of the overriding plate when the subducting lithosphere is buoyant (Experiment 4, Figs 9 and 10) or neutrally buoyant (Experiments 1 and 2, Figs 4, 5 and 7), and very little compression or extension when the subducting plate is denser than the asthenosphere (Experiments 3 and 5, Figs 5 and 10).

When asthenospheric flow is faster than plate motion the mantle flow drag force also produces tensile stress revealed by convergence

parallel extension in the subducting plate (Experiment 1, Figs 4 and 5b). However, the impact on the overriding plate is variable. For example, in Experiment 3 the mantle drag force acting on the subducted lithosphere produces a small yet noticeable convergence parallel extension of the overriding plate at 1000 s (Figs 5d and 8). However, later in the same experiment (at ∼2500 s), the subducting plate undergoes a second strong convergence parallel extension phase (Fig. 5d) while the overriding plate is submitted to convergence parallel shortening, indicating that a horizontal compressive stress is transmitted into the plate through the interplate zone.

The mantle drag force acting on the subducted slab is the integrated viscous shear stress acting between the asthenosphere and subducting lithosphere. The magnitude of this force, therefore, depends on the rate of flow in the asthenosphere, the rate of plate motion and the plate surface area. Since in our experiments, the flow rate cannot be precisely measured all around the subducting plate, we will adopt a simple measurement of the flow gradient above and below the slab to estimate the magnitude of the mantle drag force:

$$F_{\mathrm{md}} = \int_{\Sigma} \eta \left(\frac{\partial u}{\partial y} \right) W \, \mathrm{d}L, \tag{5}$$

where Σ is the contour of the slab, η the viscosity of the asthenosphere, u the velocity in the direction parallel to the slab contour while y is the direction perpendicular to the contour. W is the width of the slab and $\mathrm{d}L$ is an element of the contour. Assuming an average velocity gradient on each side (upper and lower) of the slab, the mantle drag force per slab width can be estimated as:

$$F_{\mathrm{md}} \approx \eta \left[\left(\frac{\Delta u}{\Delta y} \right)_{\mathrm{upper}} + \left(\frac{\Delta u}{\Delta y} \right)_{\mathrm{lower}} \right] L, \tag{6}$$

where L is the length of the slab from the tip to the interplate zone. The magnitude of the mantle drag force increases as the slab penetrates the mantle. In Experiment 3 at 1000 s F_{md} scales up to $\sim 7 \times 10^{12}$ N m^{-1} in nature. For comparison the slab pull force is :

$$F_{\mathrm{sp}} = \int_{\Gamma} \Delta\rho \, \mathrm{d}V, \tag{7}$$

where Γ is the volume of the slab, $\mathrm{d}V$ is an element of Γ and $\Delta\rho$ is the density difference between the slab and the surrounding mantle. Assuming that $\Delta\rho$ is constant, the slab pull force per slab width can be approximated by:

$$F_{\mathrm{sp}} \approx \Delta\rho H L, \tag{8}$$

where H is the thickness of the slab. In Experiment 3 at 1000 s (Figs 5d and 8) F_{sp} scales up to $\sim 1.5 \times 10^{13}$ N m^{-1} in nature. At 2500 s when the slab tip reaches the bottom of the tank F_{sp} has increased to $\sim 4.3 \times 10^{13}$ N m^{-1} while F_{md} has only increased to $\sim 1.3 \times 10^{13}$ N m^{-1}. This estimation confirms that, in our experiments, the slab pull force increases faster than the mantle drag force while the slab penetrates the upper mantle. This explains the slab behaviour in Experiment 4 (Fig. 9). However the slab becomes supported when reaching the upper–lower mantle boundary and, therefore, the role of the mantle drag force becomes more important. In addition to these two forces, the force balance should include the mantle drag force acting on the lower surfaces of the horizontal parts of both overriding and subducting plates as well as the push or pull exerted by the piston on the trail of the subdcuting plate. However the later cannot be precisely determined in our experiments because it changes due to the imposed constant velocity boundary condition. A detailed account of all the forces would require that the experiments are either perform with a constant stress boundary condition or that the stress between the subducting plate trail and the piston is constantly monitored during the experiment. Here we only discuss the role of the two principal forces acting on the slab, that are the slab pull force F_{sp} and the mantle drag force F_{md}.

Depending on slab geometry and flow pattern, the integrated mantle drag force is oriented downward and in the direction of the downgoing plate motion. This force results in additional normal and shear stresses on the interplate zone. However, since this zone is lubricated in our experiments we can concentrate on the consequences of the additional normal stress. When the slab dip is very steep, the mantle drag force is also steep, and can therefore, be inclined with an angle larger than the subduction zone dip angle (45° in our experiments). In this case the additional normal stress is negative and the force pulls the overriding plate towards the subducting plate. This is similar to the vertical downward action of the slab pull force (Shemenda 1994). Since the additional normal stress on the interplate zone is negative, a horizontal tensile stress is transmitted to the overriding plate, reducing the shortening rate or even producing convergence parallel extension. This corresponds to the first deformation event in Experiment 3 (Fig. 5d). The overriding plate unergoes convergence parallel extension while the dip of the slab under the interplate zone is steeper than the interplate zone (Fig. 13). When the slab dip is shallow, the resulting mantle drag force also has a shallow inclination, which can be less than the dip of the interplate zone. In this case the mantle drag force generates an additional positive normal stress on the interplate zone. The overriding plate is then submitted to an additional horizontal compressive stress, and the plate in our experiment responds with a compressional strain rate increase. This corresponds to the second deformation event in Experiment 3. The overriding plate undergoes convergence parallel contraction while the subducting plate undergoes extension when the slab dip is smaller than the interplate dipping angle (Fig. 13).

Our experimental observations thus agree with the result of statistical analysis of subduction zone parameters that the slab dip inversely correlates with the overriding plate strain regime (Lallemand *et al.* 2005) and we have proposed a physical mechanism for this observation.

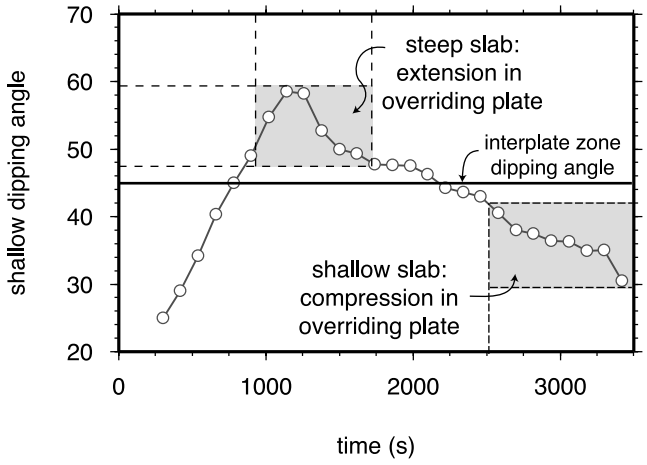

Figure 13. Evolution of the slab dip under the interplate zone in Experiment 3 (Fig. 8). The shaded areas represent the two deformation events observed at the model surface. Extensional event at ∼1000 s occurs when the slab dip is greater than the interplate zone angle (45°) while the second event (∼2500 s), which is contractional, happens when the slab dip has been reduced to values below the interplate zone dipping angle.

4.4 Limitations of the present modelling

The deformation of both plates in extension or contraction is diffuse in all our experiments. This is due to the viscous rheology adopted for the lithosphere and the assumption that overriding plate has a constant thickness. In nature the rheology of the lithosphere is more complex and allows for strain localization (Evans & Kohlstedt 1995). As shown by previous experiments, a plastic material with softening rheology results in different deformation styles with arc plate or fore-arc block subduction under compression and backarc opening under tension (Shemenda 1994; Boutelier *et al.* 2003). However, by using a viscous rheology we can visualize deformation of the plates at small stresses, whereas with plastic rheologies small stresses below the yield stress would result in no observable deformation. A constant overriding plate thickness also suppresses deformation localization. When subduction is mature, the overriding plate usually develops a volcanic arc, whose lithospheric thickness can be reduced to that of the volcanic crust alone (Stern 2002). This is, therefore, a major weak zone that focuses the deformation.

A second limitation of our models is the uniform rheology of the lithosphere during subduction. We used a constant effective viscosity thus our models do not account for viscosity reduction during subduction due to heating of the slab by the surrounding hot mantle. However, our experiments show that even a strong subducting lithosphere responds to the surrounding flow by rotating and aligning with the flow direction. Similar behaviour should be obtained when the slab is weakened during subduction, only the response should be faster. However, slab weakening might produce different slab behaviour when reaching the upper–lower mantle boundary. In Experiments 3 and 6 when the slab rolls over on the discontinuity the curvature radius is large (Figs 8 and 12). This radius should be much smaller if the viscosity of the slab tip is reduced due the high temperature. Furthermore, in Experiment 3, we imaged mantle flow passing beneath the slab before it reaches the upper–lower mantle boundary (Fig. 8c). If the slab tip was weaker it may rotate and align with flow which would change significantly the behaviour the slab during later stages and possibly prevent slab roll over.

4.5 Application to subduction in Japan

Experiment 3 with horizontal mantle flow producing a low-angle dense slab together with shortening of the overriding plate provides a new hypothesis for the subduction of the old/dense Pacific plate under the Japanese Islands. If the dynamics of this subduction system was only determined by the slab pull force and viscous resistance in the mantle, then the slab should roll back and produce extension in the overriding plate. However, spreading in the Japan Sea ended prior to 18 Ma (Gnibidenko *et al.* 1995; Tamaki 1995). It was followed by a N–S shearing episode in both Kuril and Japan that was replaced by E–W shortening at 12–15 Ma in the Sea of Japan (Jolivet *et al.* 1995). We can also rule out the absolute motion of the overriding plate as the principal cause of the shallow slab geometry and shortening of the backarc basin because the Amurian and Eurasian plates are moving slowly away from the trench. One can argue that this argument is only valid within the reference frame chosen to compute the absolute motion of the plate. We used the HS3-NUVEL1A hotspots reference frame which includes Pacific hotspots (Gripp & Gordon 2002). We acknowledge that a significantly different result is obtained using the Indo-Atlantic hotspots reference frame (O'Neil *et al.* 2005).

Our experiments reveal that westward escape flow of the Pacific mantle could maintain the shallow slab geometry despite a high slab pull force and produce shortening of the overriding plate. Whether the Pacific mantle is actually flowing under Eurasia is difficult to verify. A mantle seismic anisotropy study revealed a very large subhorizontal fast polarization axis east of the Japanese Islands between a depth of 175 and 400 km (Gung *et al.* 2003). This region may correspond to subhorizontal mantle flow in this area, but the question whether this flow supports the shallow Pacific slab, or whether shallow subduction produces subhorizontal flow remains open. Furthermore, seismic anisotropy in the mantle should be used with caution. As mentioned previously trench-parallel flow as been proposed to occur along several convergent margins based on seismic anisotropy. However, several mechanisms have been proposed for this observation: trench-parallel flow above the slab due to transpression (Mehl *et al.* 2003), or beneath the slab due to roll back (Peyton *et al.* 2001; Schellart 2004a), or trench-perpendicular flow in the wedge with 'exotic' deformation-induced lattice preferred orientation (LPO) patterns due to the presence of melts or fluids (Jung & Karato 2001; Holtzman *et al.* 2003). Furthermore, the orientation of the LPO also depends depends on the characteristic timescale of the flow (Kaminski & Ribe 2002). If the flow changes orientation too quickly the lattice prefered orientation may not reflect the direction of the flow. NNE–SSW fast directions have been observed in southern Kuril, Japan and Ryukyu (Fischer *et al.* 1998; Long & van der Hilst 2005). According to Long & van der Hilst (2005), the anisotropy is unlikely beneath the slab and since the plate convergence obliquity is small the preferred mechanism is trench-perpendicular flow in the wedge coupled with the exotic LPO. However, in view of our experiments we propose that the slab is pushed westward by the Pacific mantle and the material in the wedge accommodates this slab migration by N–S flow. This feature was not achieved in our 2-D experiments. Furthermore, we imposed an area of downward flow in our experimental tank that allowed the recycling of the mantle material through an artificial 'lower piston'. However, it is reasonable to believe that if the mantle material from the wedge is not removed by this artifice it should be extruded where possible, such as along the trench.

5 CONCLUSION

Shallow slab geometry and trench-normal shortening of the overriding plate as observed in northeast Japan could be produced by westward mantle flow escaping the shrinking Pacific plate. We have shown here that flow in the mantle with rates similar to plate motion produces a large enough overpressure on the slab lower surface to reduce a dense slab dip from 90 to 60°. Furthermore, as the slab dip reduces due to overpressure on the slab lower surface, the drag force exerted by flow in the mantle produces an additional normal stress on the interplate zone. It follows that shallow slab geometry promotes shortening of the overriding plate. This is in agreement with natural data showing that the strain regime in the overriding plate inversely correlates with the slab dip angle.

ACKNOWLEDGMENTS

Comments by L. Royden and W. Shellart on an early version and the constructive input of two anonymous reviewers and journal editors greatly improved the manuscript. Funding was provided by the University of Toronto and a Natural Sciences and Engineering Research Council of Canada Discovery Grant to A.R.C.

REFERENCES

Alvarez, W., 1982. Geological evidence for the geographical pattern of mantle return flow and the driving mechanism of plate tectonics, *J. geophys. Res.,* **87,** 6697–6710.

Alvarez, W., 1990. Geological evidence for the plate-driving mechanism: the continental undertow hypothesis and the Australian-Antarctic discordance, *Tectonics,* **9,** 1213–1220.

Alvarez, W., 2001. Eastbound sublithosphere mantle flow through the Caribbean gap and its relevance to the continental undertow hypothesis, *Terra Nova,* **13,** 333–337.

Bellahsen, N., Faccenna, C. & Funiciello, F., 2005. Dynamics of subduction and plate motion in laboratory experiments: insights into the 'plate tectonics' behavior of the Earth, *J. geophys. Res.,* **110,** doi:10.1029/2004JB002999.

Boutelier, D., Chemenda, A. & Burg, J.-P., 2003. Subduction versus accretion of intra-oceanic volcanic arcs: insight from thermo-mechanical analogue experiments, *Earth planet Sci. Lett.,* **212,** 31–45.

Buckingham, E., 1914. On physically similar systems; illustrations of the use of dimensional equations, *Phys. Rev.,* **4,** 345–376.

Cloos, M., 1993. Lithospheric buoyancy and collisional orogenesis; subduction of oceanic plateaus, continental margins, island arcs, spreading ridges, and seamounts, *GSA. Bull.,* **105,** 715–737.

Conrad, C.P. & Lithgow-Bertelloni, C., 2002. How mantle slabs drive plate tectonics, *Science,* **298,** 207–209.

Cruciani, C., Carminati, E. & Doglioni, C., 2005. Slab dip vs. lithosphere age: no direct function, *Earth planet. Sci. Lett.,* **238,** 298–310.

Doglioni, C., 1993. Geological evidence for a global tectonic polarity, *J. Geol. Soc. Lond.,* **150,** 991–1002.

Doglioni, C., Harabaglia, P., Merlini, S., Mongoli, F., Peccerillo, A. & Piromallo, C., 1999. Orogens and slabs vs. their direction of subduction, *Earth-Sci. Rev.,* **45,** 167–208.

Doglioni, C., Carminati, E. & Cuffaro, M., 2006. Simple kinematics of subduction zones, *Int. Geol. Rev.,* **48,** 479–493.

Elsasser, W.M., 1971. Sea floor spreading as thermal convection, *Geophys. Res. Lett.,* **76,** 1101–1112.

Enns, A., Becker, T.W. & Schmeling, H., 2005. The dynamics of subduction and trench migration for viscosity stratification, *Geophys. J. Int.,* **160,** 761–775.

Evans, B.K. & Kohlstedt, D.L., 1995. Rheology of rocks, in *Rock Physics and Phase Relations: A Handbook of Physical Constants, AGU Ref. Shelf* Vol. 3, pp. 148–165, ed. Aphrens, T.J., AGU, Washington, DC.

Fischer, K.M., Fouch, M.J., Wiens, D.A. & Boettcher, M.S., 1998. Anisotropy and flow in Pacific subduction zone back-arcs, *Pure appl. geophys.,* **151,** 463–475.

Forsyth, D.W. & Uyeda, S., 1975. On the relative importance of the driving forces of plate motion, *Geophys. J. R. astr. Soc.,* **43,** 13–200.

Funiciello, F., Morra, G., Regenauer-Lieb, K. & Giardini, D., 2003a. Dynamics of retreating slabs: 1. Insights from two-dimensional numerical experiments, *J. geophys. Res.,* **108,** doi:10.1029/2001JB000898.

Funiciello, F., Faccenna, C., Giardini, D. & Regenauer-Lieb, K., 2003b. Dynamics of retreating slabs: 2. Insights from three-dimensional laboratory experiments, *J. geophys. Res.,* **108,** doi:10.1029/2001JB000896.

Funiciello, F., Moroni, M., Piromallo, C., Faccenna, C., Cenedese, A. & Bui, H., 2006. Mapping mantle flow during retreating subduction: laboratory models analyzed by feature tracking, *J. geophys. Res.,* **111,** doi:10.1029/2005JB003792.

Garfunkel, Z., 1975. Growth, shrinking, and long-term evolution of plates and their implications for flow pattern in the mantle, *J. geophys. Res.,* **80,** 4425–4432.

Garfunkel, Z., Anderson, C.A. & Schubert, G., 1986. Mantle circulation and the lateral migration of subducted slabs, *J. geophys. Res.,* **91,** 7205–7223.

Gnibidenko, H.S, Hilde, T.W.C., Gretskaya, E.V. & Andreyev, A., 1995. Kuril (South Okhotsk) backarc basin, in *Backarc Basins: Tectonics and Magmatism,* pp. 441–449, ed. Taylor, B., Plenum Press, New York.

Griffiths, R., Hackney, R. & van der Hilst, R., 1995. A laboratory investigation of the effects of trench migration on the descent of subducted slabs, *Earth planet. Sci. Lett.,* **133,** 1–17.

Gripp, A.E. & Gordon, R.G., 2002. Young tracks of hotspots and current plate velocities, *Geophys. J. Int.,* **150,** 321–361.

Gudmundsson, O. & Sambridge, M., 1998. A regionalized upper mantle (RUM) seismic model, *J. geophys. Res.,* **103,** 7121–7136.

Guillou-Frottier, L., Buttles, J. & Olson, P., 1995. Laboratory experiments on the structure of subducted lithosphere, *Earth planet. Sci. Lett.,* **133,** 19–34.

Gung, Y., Panning, M. & Romanowicz, B., 2003. Global anisotropy and the thickness of continents, *Nature,* **422,** 707–710.

Heki, K. *et al.*, 1999. The Amurian plate motion and current plate kinematics in eastern Asia, *J. geophys. Res.,* **104,** 29 147–29 155.

Heuret, A. & Lallemand, S., 2005. Plate motions, slab dynamics and back-arc deformation, *Phys. Earth planet Inter.,* **149,** 31–51.

Heuret, A., Funiciello, F., Faccenna, C. & Lallemand, S., 2007. Plate kinematics, slab shape and back-arc stress: a comparison between laboratory models and current subduction zones, *Earth planet. Sci. Lett.,* **256,** 473–483.

Holtzman, B.K., Kohlstedt, D.L., Zimmerman, M.E., Heidelbach, F., Hiraga, T. & Hustoft, J., 2003. Melt segregation and strain partitioning: implications for seismic anisotropy and mantle flow, *Science,* **301,** 1227–1230.

Jarrard, R.D., 1986. Relations among subduction parameters, *Rev. Geophys.,* **24,** 217–284.

Johnston, S.T. & Thorkelson, D.J., 1997. Cocos-Nazca slab window beneath Central America, *Earth planet Sci. Lett.,* **146,** 465–474.

Jolivet, L., Shibuya, H. & Fournier, M., 1995. Paleomagnetic rotations and the Japan Sea opening, in *Active Margins and Marginal Basins of the Western Pacific,* pp. 355–369, eds Taylor, B. & Natland, J., AGU, Washington.

Jung, H. & Karato, S.I., 2001. Water-induced fabric transitions in olivine, *Science,* **293,** 1460–1463.

Kaminski, E. & Ribe, N.M., 2002. Timescales for the evolution of seismic anisotropy in mantle flow, *Geochem. Geophys. Geosyst.,* **3,** doi:10.1029/2001GC000222.

Karato, S. & Wu, P., 1993. Rheology of the upper mantle: a synthesis, *Science,* **260,** 771–778.

Lallemand, S., Heuret, A. & Boutelier, D., 2005. On the relationships between slab dip, back-arc stress, upper plate absolute motion, and crustal nature in subduction zones, *Geochem. Geophys. Geosyst.,* **6,** doi:10.1029/2005GC000917.

Long, M.D. & van der Hilst, R.D., 2005. Upper mantle anisotropy beneath Japan from shear wave splitting, *Phys. Earth planet. Inter.,* **151,** 206–222.

Martinod, J., Funiciello, F., Faccenna, C., Labanieh, S. & Regard, V., 2005. Dynamical effects of subducting ridges: insights from 3-D laboratory models, *Geophys. J. Int.,* **163,** 1137–1150.

Mehl, L., Hacker, B.R., Hirth, G. & Kelemen, P.B., 2003. Arc-parallel flow within the mantle wedge: evidence from the accreted Talkeetna arc, south central Alaska, *J. geophys. Res.,* **108,** doi:10.1029/2002JB002233.

Mitrovica, J.X. & Forte, A.M., 2004. A new inference of mantle viscosity based upon joint inversion of convection and glacial isostatic adjustment data, *Earth planet Sci. Lett.,* **225,** 177–189.

Nelson, T.H. & Temple, P.G., 1972. Mainstream mantle convection: a geologic analysis of plate motion, *Am. Assoc. Petrol. Geol. Bull.,* **56,** 226–246.

Olbertz, D., Wortel, J.R. & Hansen, U., 1997. Trench migration and subduction zone geometry, *Geophys. Res. Lett.,* **24,** 221–224.

O'Neill, C., Müller, D. & Steinberger, B., 2005. On the uncertainties in hot spot reconstructions and the significance of moving hot spot reference frames, *Geochem. Geophys. Geosyst.,* **6,** doi:10.1029/2004GC000784.

Peyton, V., Levin, V., Park, J., Brandon, M., Lees, J., Gordeev, E. & Ozerov, A., 2001. Mantle flow at a slab edge; seismic anisotropy in the Kamchatka region, *Geophys. Res. Lett.,* **28,** 379–382.

Pysklywec, R.N. & Ishii, M., 2005. Time dependent subduction dynamics driven by the instability of stagnant slabs in the transition zone, *Phys. Earth planet. Inter.,* **149,** 115–132.

Pysklywec, R.N., Mitrovica, J.X. & Ishii, M., 2003. Mantle avalanches as a driving force for tectonic reorganization of the southwest Pacific, *Earth planet Sci. Lett.,* **209,** 29–38.

Royden, L.H. & Husson, L., 2006., Trench motion, slab geometry and viscous stresses in subduction systems, *Geophys. J. Int.,* **167,** 881–905.

Russo, R.M. & Silver, P.G., 1994. Trench-parallel flow beneath the Nazca plate from seismic anisotropy, *Science,* **263,** 1105–1111.

Schellart, W.P., 2004a., Quantifying the net slab pull force as a driving mechanism for plate tectonics, *Geophys. Res. Lett.,* **31,** doi:10.1029/2004GL019528.

Schellart, W.P., 2004b., Kinematics of subduction and subduction-induced flow in the upper mantle, *J. geophys. Res.,* **109,** doi:10.1029/2004JB002970.

Schellart, W.P., 2005. Influence of the subducting plate velocity on the geometry of the slab and migration of the subducting hing, *Earth planet Sci. Lett.,* **231,** 197–219.

Schellart, W.P., Freeman, J., Stegman, D.R., Moresi, L. & May, D., 2007. Evolution and diversity of subduction zones controlled by slab width, *Nature,* **446,** 308–311, doi:10.1038/nature05615.

Scholtz, C.H. & Campos, J., 1995. On the mechanism of seismic decoupling and back arc spreading at subduction zones, *J. geophys. Res.,* **100,** 22 103–22 115.

Scoppola, B., Boccaletti, D., Bevis, M., Carminati, E. & Doglioni, C., 2006. The westward drift of the lithosphere: a rotational drag?, *GSA Bull.,* **118,** 199–209.

Shemenda, A.I., 1994. *Subduction: Insights from Physical Modelling,* pp. 207, Kluwer Academic Publishers, Dordrecht.

Stegman, D.R., Freeman, J., Schellart, W.P., Moresi, L. & May, D., 2006. Influence of trench width on subduction hinge retreat rates in 3-D models of slab rollback, *Geochem. Geophys. Geosyst.,* **7,** doi:10.1029/2005GC001056.

Stern, R.J., 2002. Subduction zones, *Rev. Geophys.,* **40,** doi:10.1029/2001RG000108.

Tamaki, K., 1995. Opening tectonics of the Japan sea, in *Backarc Basins: Tectonics and Magmatism,* pp. 407–420, ed. Taylor, B., Plenum Press, New York.

Taira, A., 2001. Tectonic evolution of the Japanese island arc system, *Annu. Rev. Earth Planet.,* **29,** 109–34.

Uyeda, S. & Kanamori, H., 1979. Back-arc opening and the mode of subduction, *J. geophys. Res.,* **84,** 1049–1061.

Winder, R.O. & Peacock, S.M., 2001. Viscous forces acting on subducting lithosphere, *J. geophys. Res.,* **106,** 21 937–21–951.

Zhong, S. & Gurnis, M., 1995. Mantle convection with plates and mobile, faulted plated margins, *Science,* **267,** 838–843.